

Fano fluctuations in superconducting nanowire single-photon detectors

A. G.Kozorezov¹, C. Lambert¹, F. Marsili², M. J. Stevens³, V. B. Verma³, J.P.Allmaras², M. D. Shaw², R. P. Mirin³, Sae Woo Nam³

¹*Department of Physics, Lancaster University, Lancaster, UK,*

²*Jet Propulsion Laboratory, California Institute of Technology,
4800 Oak Grove Dr., Pasadena, California 91109, USA,*

³*National Institute of Standards and Technology, 325 Broadway, Boulder, CO 80305, USA*

(Dated: February 10, 2017)

Because of their universal nature, Fano fluctuations are expected to influence the response of superconducting nanowire single-photon detectors (SNSPDs). We predict that photon counting rate (PCR) as a function of bias current (I_B) in SNSPDs is described by an integral over a transverse coordinate-dependent complementary error function. The latter describes smearing of local responses due to Fano fluctuations of the amount of energy deposited into electronic system. The finite width, σ , of the PCR vs I_B arises from fluctuations in the energy partition between quasiparticles and phonons during the energy down-conversion cascade. In narrow-nanowire SNSPDs the local responses are uniform, and the effect of Fano-fluctuations on σ is dominant. In wide-nanowire SNSPDs with strong coordinate dependence of local responses due to vortex-antivortex unbinding and vortex entry from edges, Fano-fluctuations smear singularities imprinted by vorticity on the transition part of PCR curve. We demonstrate good agreement between theory and experiments for a series of bath temperatures and photon energies in narrow-wire WSi SNSPDs. The time-resolved hotspot relaxation curves predicted by Fano fluctuations match the Lorentzian shapes observed in experiments over the whole range of bias currents investigated except for their tails .

I. INTRODUCTION

The conversion of light into detectable excitations constitutes the key process in photodetection. Energy flow and relaxation pathways are the central topic which is equally interesting in many areas from traditional scintillators¹ or new graphene-based materials^{2,3}. The efficiency of detection depends on competition between different energy flow pathways.

Fano fluctuations describe variations in the number of charge carriers generated in a single-particle or single-photon sensor. Upon impact with a particle or absorption of a photon, energy is deposited in the sensor. This energy is partitioned between charged and neutral elementary excitations, for example between electrons and phonons. Fano fluctuations are caused by the branching processes and result in variations in the fraction of energy deposited in each system. Fano fluctuations are known to determine the theoretical limit of spectral resolution of many types of spectrometers, and are a limiting factor in the noise characteristics of CCDs and CMOS image sensors^{4,5}, as well as superconductor sensors such as superconducting tunnel junctions and microwave kinetic inductance detectors^{6,7}. Fano fluctuations may also be significant in sensors lacking an energy gap in the spectrum of elementary excitations, for example in superconducting transition edge microcalorimeters grown on a solid substrate⁸⁻¹⁰ and magnetic microcalorimeters^{11,12}. The relevant parameter of the detector material is the Fano factor, which quantifies the branching variance: a smaller factor indicates better resolving power.

To date, the role of Fano fluctuations in SNSPDs has not been discussed in the literature, likely because it was viewed as irrelevant. It has generally been as-

sumed that an ideal SNSPD should exhibit sharp spectral and current thresholds for photodetection, characterized by a step function in detection efficiency when plotted as a function of bias current¹³. The broadening of this step function into the sigmoidal shape observed in experiments has been attributed to inhomogeneities in nanowire width or thickness, or to variations in the position of the photon absorption site affecting vortex entry at the edge of the wire competing with unbinding of vortex-antivortex pairs away from the edge¹⁴⁻²².

Here, we present a study of the influence of Fano fluctuations on the current and spectral dependence of the detection efficiency of SNSPDs. We found that a sigmoidal shape is expected even in the absence of these inhomogeneities. We show that the energy deposited into the electronic system by monochromatic photons fluctuates about the mean value due to the partition between quasiparticles (QP) and phonons. This occurs during energy down-conversion, with a variance given by the Fano factor. We show that photon counting rate vs. bias current in SNSPDs in general is described by an integral over transverse coordinate-dependent complementary error function with a width σ determined by variance of Fano fluctuations.

II. FANO FLUCTUATIONS IN SNSPDS

A. Energy down-conversion cascade

We start by describing the first moments following the absorption of a photon in the SNSPD. We adapt the picture of energy down-conversion developed in our early work²³ for a thin, disordered metal film. Fig.1 schemat-

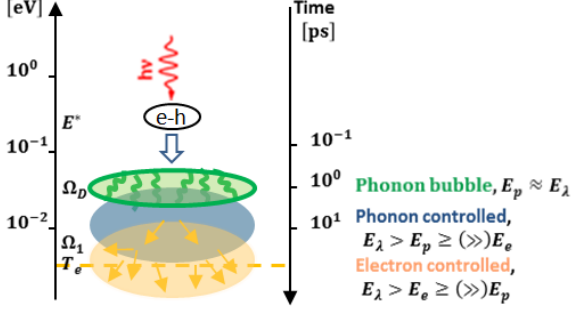


FIG. 1: Schematic picture of photoelectron-hole energy down-conversion cascade in a metal

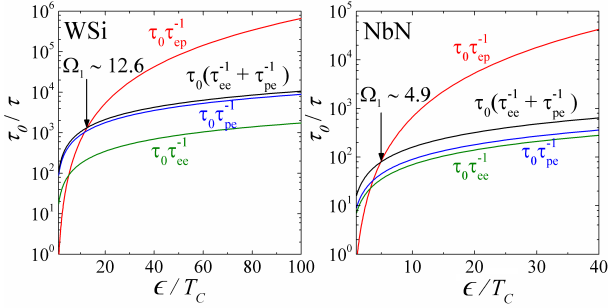


FIG. 2: Electron-electron, τ_{ee} , electron-phonon, τ_{ep} , and phonon-electron, τ_{pe} , scattering-out times vs excitation energy in WSi and NbN.

ically illustrates the evolving down-conversion cascade. At $t = 0$, a photon is absorbed and an electron-hole pair is generated. The sum of electron and hole energies is the energy of a photon, E_λ . On average half this energy is given to the electron and half to the hole. The energy and time scales in Fig.1 are given to illustrate an absorption of optical photon. E_1^* is the threshold energy separating the higher-energy interval, where electron-electron scattering with large momentum transfer dominates inelastic relaxation of the electron(hole) due to electron-phonon interaction. For excitations of energy $\epsilon < E_1^*$ the electron-phonon interactions totally dominate both the phonon-electron and electron-electron interactions until the mean energies of interacting electrons and phonons reach a lower threshold, Ω_1 , below which electron-electron and phonon-electron interactions in the disordered film dominate. Usually $\Omega_1 \ll \Omega_D$, where Ω_D is the Debye energy. Fig.2 shows scattering-out relaxation times as a function of quasiparticle energy calculated from Fermi energy over the range of energies up to Debye energy. Electron-electron scattering time as a function of energy was calculated from Altshuler and Aronov's formula for a disordered 2D normal metal²⁴, while electron-phonon and phonon-electron scattering times were taken from Chang²⁵. It is important to note that the expressions for electron-phonon

and phonon-electron times were taken neglecting vertex renormalisation by strong disorder, which is valid for the range of energies $\epsilon l/\hbar c \geq 1$, where l is the elastic mean free path for electrons and c - is the sound velocity^{26,27}. This inequality holds true for higher energies, while at lower energies, close to Ω_1 , the role of disorder becomes important. The characteristic time τ_0 is taken for WSi and NbN to be 5-10 and 0.3-0.6 ns respectively, which falls into the expected range for the clean limit, consistent with the magnitude of the Debye and critical temperatures if the median value of these is taken as the effective coupling strength²⁸. As follows from Fig.2, in both NbN and WSi the electron-phonon interaction dominates the electron-electron scattering rate over a significant spectral range. This means that the loss of high frequency non-equilibrium (athermal) phonons from the thin film, with thickness comparable to the phonon mean free paths, may be significant.

Using the estimate for electron-electron scattering-out time for large momentum transfers for $\epsilon > \Omega_D$, we obtain that $\tau_{ee}(\epsilon) > \tau_{ep}(\epsilon > \Omega_D) = \tau_s$ for $\epsilon < E_1$ with E_1 close to 1 eV²³. The energy loss for electron/hole of the initial pair due to electron-electron interactions with electrons of the Fermi distribution at equilibrium is slower. It can be roughly estimated from the expression for $\tau_{ee}^{out}(\epsilon)$ ²⁴

$$\begin{aligned} \frac{1}{\tau_{ee}^{out}(\epsilon)} &\propto \int_0^\epsilon d\omega \int_0^\omega d\epsilon' \int_0^\infty dq q^2 W_q \frac{1}{qV_F} \\ \dot{\epsilon} &\propto \int_0^\epsilon d\omega \omega \int_0^\omega d\epsilon' \int_0^\infty dq q^2 W_q \frac{1}{qV_F} \\ \dot{\epsilon} &= -\frac{2}{3} \frac{\epsilon}{\tau_{ee}^{out}(\epsilon)} \end{aligned} \quad (1)$$

where ω and q are the energy and momentum transfer at the collision, ϵ' is the energy of a particle the electron collides with, W_q is the matrix element describing the interaction, V_F is Fermi velocity. Solving the last equation yields

$$\frac{\epsilon(t)}{\epsilon_0} = \left[1 + \frac{4}{3} \frac{t}{\tau_{ee}^{out}(\epsilon_0)} \right]^{-1/2} \quad (2)$$

where $\epsilon_0 = \epsilon(0)$. The energy of an electron excited at ϵ as follows from (2) halves at $9/4\tau_{ee}^{out}(\epsilon)$. The loss of half of the energy due to sequential emission of phonons takes $\sim (\epsilon/2\Omega_D)\tau_s$. Both rates are equal at E_1^* , $E_1^* = E_1 \left(\frac{9\Omega_D}{2E_1} \right)^{1/3}$. For $\Omega_1 < \epsilon < E_1^*$ the electron-phonon scattering is the dominant mechanism of electron/hole energy relaxation. With $E_1 \sim 1$ eV and $\Omega_D \sim 30$ meV we obtain for typical materials $E_1^* \sim 500$ meV. When the energy of initial electron/hole (or secondary excitations) is close to E_1^* their subsequent cooling proceeds mostly via sequential emission of phonons. Since the characteristic values for τ_s are tens of fs, unless the materials have a small Debye energy, cooling from 500 meV down to Ω_D will last a fraction of a picosecond.

By the end of it, which completes before the lifespan of the first emitted phonons, most of the photon energy has been transferred to high energy (Debye) phonons. It is convenient to consider this highly non-equilibrium state as the natural initial condition for the subsequent evolution of interacting quasiparticles and phonons. In Fig.1 this condition is called a phonon bubble.

B. Modelling Fano-fluctuation

We consider a simple model of photon detection^{30,31}. Following the absorption of a photon of energy E_λ , a fraction of the energy, $E < E_\lambda$, is deposited into electronic excitations. During the energy down-conversion cascade, a hotspot is created²³. For a narrow and thin wire we assumed that the hotspot spans the width of the wire, W , occupying volume $V_{HS} = WL_{HS}d$, with $L_{HS} \geq W$ being its length along the wire and d is the wire thickness. In this situation L_{HS} can be determined in tomography experiments³⁰. We assume that after completion of the cascade the quasiparticle distribution is thermalized owing to a strong electron-electron interaction in a disordered nanowire. Therefore, we assumed that after the absorption of a photon the QP temperature instantly increased from bath temperature, T_b , to excitation temperature, T_{ex} . The hotspot excitation temperature is determined from the thermal balance

$$E_{HS}(I_B, T_{ex}, B) - E_{HS}(I_B, T_b, B) = \int_{T_b}^{T_{ex}} dT' C(T', I_B, B) = E_{HS}^{QP}(I_B, T_{ex}, B) - E_{HS}^{QP}(I_B, T_b, B) + 2N(0)V_{HS}k_B \int_{-\infty}^{\infty} d\xi \int_{T_{ex}^{-1}}^{T_b^{-1}} d\beta \frac{1}{\exp(\beta\epsilon) + 1} \frac{\partial \epsilon}{\partial \beta} = E \quad (3)$$

where $E_{HS}(I_B, T, B)$ is the internal energy of the hotspot, $N(0)$ is the normal state density of states at the Fermi level, $\epsilon = \sqrt{\xi^2 + \Delta^2(I_B, T, B)}$ is the quasiparticle energy, Δ is the order parameter in current carrying nanowire, B is the external magnetic field and E the actual amount of energy deposited in the electronic system.

$$E_{HS}^{QP}(I_B, T, B) = 4N(0)V_{HS} \int_0^\infty d\epsilon \frac{\epsilon \rho(\epsilon, I_B, T, B)}{\exp(\epsilon/T) + 1} \quad (4)$$

Here $\rho(\epsilon, T, I_B, B)$ is the density of states within the hotspot in units of $N(0)$. The dependencies on bias current I_B , temperature T and magnetic field B originate from the pair-breaking energy and the order parameter being functions of T , I_B and B . The last term in the expression (3) originates from the dependence of QP dispersion relations in the hotspot on temperature.

In an ideal SNSPD there is a count event every time the energy E exceeds the threshold E^* , determined from

$$E_{HS}(I_B, T_b, B) + E^* = E_{HS}(I_B, T_s, B) \quad (5)$$

where T_s is the temperature at which the hotspot undergoes transition from the superconducting to the normal

state. This temperature depends on bias current and external magnetic field and can be found for a narrow wire using the solution of the Usadel equation for density of states³² and the dependence of the order parameter on current, temperature and magnetic field^{30,31}.

In wider wires the characteristic shape of a hotspot is more complicated. If the photon absorption site is not close to the edge of the wire, then the hotspot is cylindrical. Its radius, R_{HS} , is smaller than its width, $W > R_{HS} \gg d$, the hotspot does not span the wire width, and its creation results in a current density redistribution. The latter depends on the lateral coordinate of the absorption site, \mathbf{r} (2-dimensional geometry). Finally, in very thick wires the hotspot may be spherical (or close to semi-spherical for shallow absorption), with the radius $R_{HS} \ll \min\{d, W\}$. The geometry of current flow in this wide and thick nanowire becomes 3-dimensional.

In wide thin nanowires, the change in the current flow facilitates vortex entry at the edges of the nanowire or unbinding of vortex-antivortex pairs. In this situation, Fano fluctuations result in supercurrent density fluctuations and their description becomes more complicated. The fluctuating order parameter, current density and temperature in the hotspot become dependent on the coordinate of the absorption site and are connected through a more complicated relation. The coordinate-dependent detection current, $I_{det}(y, E, T_b, B, \lambda)$ is introduced through the appropriate simulation^{15,18}, and the implicit condition for the E^* threshold to trigger the detection click can be written as

$$I_B = I_{det}(y, T^*, T_b, B, \lambda) = I_{det}(y, E^*, T_b, B, \lambda) \quad (6)$$

where $T^* = T(E^*)$ is the threshold temperature of the hotspot corresponding to energy deposition E^* .

The normalised probability distribution $P(E)$ describing energy deposition into the electronic system is Gaussian, $\int_{-\infty}^{\infty} dE P(E) = 1$,

$$P(E) = \frac{1}{\sqrt{2\pi}\sigma} \exp\left[-\frac{(E - \bar{E})^2}{2\sigma^2}\right] \quad (7)$$

The distribution is centered around a mean value $\bar{E} = \bar{\chi}E_\lambda$, where $\bar{\chi} < 1$, $\chi = E/E_\lambda$ is the photon yield, which we defined as the ratio of the energy deposited in the hotspot after the absorption of the photon (E) to the photon energy (E_λ). The full width at half maximum of the distribution $P(E)$ is $2\sqrt{2\ln 2}\sigma$, where σ is the variance. Since a count occurs when $E \geq E^*$, simple integration yields the normalised PCR for a narrow wire in the form

$$PCR^{NW} = \int_{E^*}^{\infty} dE P(E) = \frac{1}{2} \operatorname{erfc}\left(\frac{E^* - \bar{E}}{\sqrt{2}\sigma}\right) = \frac{1}{2} \operatorname{erfc}\left[\frac{E(I_B, T_s, B) - E(I_B, T_b, B) - \bar{E}}{\sqrt{2}\sigma}\right] \quad (8)$$

For a wide wire the photon count occurs if the bias current exceeds the minimum of detection current, which

is a function of the coordinate y across the wire and depends on hotspot temperature (deposited energy), bath temperature, magnetic field, photon wavelength, $I_{det}(y, T(E), T_b, B, \lambda) = I_{det}(y, E, T_b, B, \lambda)$. In this situation

$$PCR^{WW} = \int_0^\infty dEP(E) \frac{1}{W} \int_{-W/2}^{W/2} dy \Theta [I_B - I_{det}(y, E, T_b, B, \lambda)] = \int_0^\infty dEP(E) w(E, T_b, B, \lambda) = \frac{1}{W} \int_{-W/2}^{W/2} dy \operatorname{erfc} \left[\frac{I_B - I_{det}(y, \chi E_\lambda, T_b, B, \lambda)}{\sqrt{2\sigma I'_{det}(y, \chi E_\lambda, T_b, B, \lambda)}} \right] \quad (9)$$

where $\Theta(x)$ is the Heaviside function, $w(T(E), T_b, B, \lambda)$ is the fraction of the wire width where generation of a vortex results in formation of a normal domain across the wire, and $I'_{det}(y, \chi E_\lambda, T_b, B, \lambda) = \partial I'_{det}(y, E, T_b, B, \lambda) / \partial E|_{E=\chi E_\lambda}$. In wide nanowires, the expression (9) must be further convolved if the light polarization results in a spatial profile of the absorption sites.

The variance is determined from two statistically independent processes as $\sigma^2 = \sigma_1^2 + \sigma_2^2$. Following photon absorption, a rapid process of energy down-conversion is initiated, engaging numerous electronic and phonon excitations. Phonons can be divided into two groups. Non-pair-breaking phonons with energy $\hbar\Omega$ smaller than twice the order parameter 2Δ are decoupled from the condensate and can only be reabsorbed by excited QPs. In thin films we neglect their reabsorption, assuming the re-absorption time to be considerably longer than their escape into a substrate or thermalization time. In contrast, higher energy phonons can break Cooper pairs and exchange energy with the electronic system. In a bulk superconductor, if the distance from the absorption site to escape interface far exceeds the phonon mean free path, none of the pair-breaking phonons escapes into the thermal bath before QPs thermalise. By the end of down-conversion the energy of a photon splits between QPs and non-pair-breaking phonons. σ_1 describes statistical fluctuations of E originating from fluctuations of numbers of pair-breaking phonons under the assumption that none of the pair-breaking phonons from the down-conversion cascade escapes. It can be written $\sigma_1^2 = F\varepsilon E$, where 2ε is the mean energy which is necessary to spend in order to generate one pair of QPs. In superconducting films with thickness comparable to the mean free path of pair-breaking phonons, some of the highly energetic (athermal) phonons will escape. Thus, instead of E we must write $E' = (1 - \chi_a)E$, where we introduce $0 < \chi_a < 1$ to account for the average fraction of athermal phonons escaping from the nanowire prior to random partition of energy between QPs and non-pair-breaking phonons, which are de-coupled from condensate. The Fano factor in most superconductors is $F \simeq 0.2^{6,7}$.

The energy loss from the film due to escaping athermal phonons is a random process, depending on mean free paths of phonons and transmission characteristics

into the substrate. Therefore, there appears the second independent contribution to the variance, σ_2 . If all athermal phonons are re-absorbed in the film, which is the case for thick films illuminated from the top, then $\chi_a = 0$ and $\sigma_2 = 0$ while $\sigma_1^2 = F\varepsilon E$ becomes the known Fano fluctuations variance. σ_2 originates from fluctuations in the transmission of athermal phonons to the substrate^{9,10}: $\sigma_2^2 = J(E_\lambda)\varepsilon E_\lambda$, we call this contribution phonon down-conversion noise. This contribution to Fano noise has also been expressed in conventional form³³ with the factor $J(E_\lambda)$. The accurate determination of Fano-factor $J(E_\lambda)$ is not an easy problem. It involves evaluation of statistical fluctuations of loss of successive generations of athermal phonons, which are part of evolving distribution of the down-conversion process. We may, however, derive the lower limit to $J(E_\lambda)$. While lower-energy longer-living phonons from later generations account for the majority of energy loss, the opposite is true for fluctuations of energy loss. With multiplication of phonon numbers and decrease of their mean energy, the relative fluctuation of energy loss from phonons from later-generations decreases. We estimate the contribution to $J(E_\lambda)$ from phonons of first generation (phonon bubble) designating it $J^1(E_\lambda)$ and ignore contributions from subsequent athermal phonon generations arriving in the lower limit, $J^1(E_\lambda) < J(E_\lambda)$.

In a thin film, photons are absorbed homogeneously through the depth of the film, and, similarly, phonons of the first generation (phonon bubble) are also homogeneously generated while the energetic photoelectron(hole) performs a random walk in the film. Thus, taking the limit $d \rightarrow 0$ and $m = 0$ we simplify the expression for $J^1(E_\lambda)$, which was derived in earlier work³³ and obtain

$$J^1 = 2 \frac{\Omega_D}{\varepsilon} \frac{l_{pe,D}}{d} \int_{\cos(\theta_c)}^1 d\xi \xi \eta(\xi) \left\{ \frac{1}{4} \left(\frac{l_{pe,D}}{d} \right)^4 - \int_0^{d/l_{pe,D}\xi} dx x^3 \left[e^{-x} + \frac{1}{2} \eta(\xi) \sin^2(\theta_c/2) (1 - e^{-2x}) \right] \right\} \quad (10)$$

Here θ_c is the angle of total internal reflection, so that phonons that impinge the escape interface at larger angles stay inside the plane parallel film until they undergo scattering-assisted conversion and move at smaller angles $\theta < \theta_c$, η is the phonon transmission coefficient through the interface with the substrate for incidence below the critical angle, and $l_{pe,D}$ is the mean free path of Debye phonons with respect to absorption by electrons. This result has the following meaning. The variance of the number of phonons emitted into the critical cone from any energy interval follows a binomial distribution. The contributions from phonons of different energies are statistically independent. Therefore, total variance is the sum (integral) of contributions from individual groups of phonons of the flat distribution of phonons of the first generation. Individual factors in the expression (10) reflect: Ω_D - the dominant phonon energy in the phonon

bubble, $\frac{l_{pe,D}}{d}$ - probability of survival until reaching the escape interface, the inner integral - averaging phonon contributions over their distribution, accounting for their probabilities to reach the interface depending on energy and angle of incidence within the critical cone. Note that a binomial distribution is close to a normal distribution in expression (7) under the assumption of large phonon numbers in each energy interval. Thus, integration over the spectrum works well for phonons of later generations. For first-generation phonons it works for the dominant phonon group with energies close to Debye energy, and the second integral in (10) is an approximation of the dominant phonon contribution.

The total variance due to Fano noise can be written as $\sigma^2 = F_{eff}\varepsilon E\lambda$, where the effective Fano-factor is $F_{eff} = F(1 - \chi_a) + J$. Our estimate of J relies on using the simplest model of one phonon-mode with a linear dispersion relation (Debye) approximation. For phonons of the first few generations we have $\epsilon l/\hbar c \geq 1$, and our estimate of J^1 is not affected by disorder. Given these approximations this estimate provides only a rough indication of the magnitude of the effect.

In the next section we compare our simulation with experiments on WSi SNSPDs. Because of the large acoustic mismatch between WSi (W_3Si) and the SiO_2 substrate, even for normal incidence we have $\chi \leq 0.5$. Taking $\chi = 0.5$ for WSi on amorphous SiO_2 substrate we obtain $1.0 \leq J \leq 1.5$ for $5 \leq \tau_0 \leq 10$ ns. For NbN on SiO_2 , a similar calculation yields $0.8 \leq J \leq 1.0$ for $0.5 \leq \tau_0 \leq 1.0$ ns. With these estimates we conclude that phonon down-conversion noise even due to phonons of the first generation dominates Fano fluctuations, $\sigma_2 \gg \sigma_1$. This is not surprising because the fluctuations of the number of phonons falling within the escape cone and the fluctuations of ultimate number of quasiparticles are both proportional to the square root of the respective mean numbers. Fluctuations for athermal phonons are strong, partly because of their large energy and hence smaller numbers, but more importantly because only a significantly smaller fraction of all athermal phonons (those within the escape cone) contribute to fluctuations in the corresponding energy loss. The subsequent phonon generations also contribute to fluctuations increasing σ_2 , although each subsequent contribution becomes smaller, because of the twofold increase of the number of phonons with every generation. Thus, even if we overestimated J^1 , there is still an extra contribution due to lower energy phonons, so that most probably $\sigma_2 \gg \sigma_1$. Because we cannot provide credible estimates for contributions to overall variance from later phonon generations we will use F_{eff} as a fitting parameter. The likely range of variation of F_{eff} must be consistent with our estimate for J^1 .

C. The effect of Fano-fluctuations on the shape of PCR curves in narrow, homogeneous SNSPDs

The shape of PCR curve vs bias current at fixed values of external parameters T , λ , B is affected by the bias dependence of the energy terms in the numerator of the argument of the complimentary error function in equation (8), i.e $E(I_B, T_s, B) - E(I_B, T_b, B) - \bar{E}$. Also in the current-carrying superconductor both variances σ_1 and σ_2 depend on I_B . σ_1 depends on the order parameter at critical point Δ_s , while σ_2 due to contributions of phonons of later generations may weakly depend on the threshold energy Ω_1 , because both Δ_s and Ω_1 depend on I_B . We defined the cutoff current of the SNSPD at fixed wavelength, bath temperature, and magnetic field, $I_{co}(\lambda, T_b, B)$, as the inflection point of the PCR vs I_B curve and used the approximation $E(I_B, T_s, B) - E(I_B, T_b, B) - \bar{E} \approx \alpha^{-1}(I_B, \lambda, T_b, B)(I_B - I_{co}(\lambda, T_b, B))$ to obtain

$$PCR = \frac{1}{2} \operatorname{erfc} \left[\frac{I_B - I_{co}(\lambda, T_b, B)}{\sqrt{2}\sigma(I_B, T_b, B)\alpha(I_B, \lambda, T_b, B)} \right] \quad (11)$$

This is the modification of the equation (9) for the case of a narrow wire with a detection current, that is not dependent on y -coordinate across the wire. As seen from (11), PCR as a function of bias current differs from the ideal complimentary error function because of the current dependence of α and σ in the denominator. If the width of the PCR curve is small relative to de-pairing current, we may keep only the first term in series expansion of $E(I_B, T_s, B) - E(I_B, T_b, B) - \bar{E}$. This corresponds to α being independent of bias current. Similarly, if the width of the PCR curve is small relative to the de-pairing current, the dependence of σ on bias current can also be neglected. Therefore, deviations of PCR from an ideal complimentary error function reflect either the specific features of Fano-fluctuations in the current-carrying superconducting nanowire (through σ) or strong non-linearity of the SNSPD response (through α).

The down-conversion in a strongly disordered current-carrying nanowire is different from typical superconducting sensors with no significant disorder, such as superconducting tunnel junctions and many types of microwave kinetic inductance detectors. In these detectors, the temperature of the hotspot does not rise close to the critical temperature T_C even for photon energies as high as a few keV. The transport current is small compared to the de-pairing current and the order parameter stays close to its zero current-temperature value. Therefore, the energy required to generate a quasiparticle is constant during the downconversion process, $\varepsilon = 1.75\Delta(0)$. By contrast, in an SNSPD at the edge of the transition to the normal state, the temperature of the hotspot reaches the critical value T_s , while the order parameter remains nonzero at the level $\Delta(I_B, T_s)$, but is significantly smaller than its zero temperature value for a given bias current. As a result, some of the non-pair-breaking phonons with energies below $2\Delta(t)$ that were emitted shortly after

photon absorption regain their pair-breaking capability later, when their energy starts exceeding the decreasing $2\Delta(t)$. This happens if down-conversion and thermalisation times are faster than phonon escape time from the film. In this asymptotic limit $\varepsilon = 1.75\Delta(T_s)$, and it decreases with bias current, while T_s increases^{30,31}. The corresponding σ_1 also decreases, resulting in a steeper rise of the *PCR* vs I_B . The dependence of the second contribution σ_2 on I_B is weaker, reflecting the fact that σ_2 is the contribution from the initial generations of excitations when the order parameter is much less affected. Therefore, to experimentally observe the bias dependence of the variance σ , σ_1 and σ_2 must be comparable in magnitude. This situation is easier to fulfil in larger gap NbN than in WSi.

The other factor, α , depends on bias current considerably stronger, because it is determined by a highly non-linear function of bias current $E(I_B, T_s, B) - E(I_B, T_b, B) - \bar{E}$, $\alpha^{-1}(I_B, \lambda, T_b, B) = \frac{\partial(E(I_B, T_s, B) - E(I_B, T_b, B))}{\partial I_B} \Big|_{\bar{\chi}E\lambda}$ (neglecting potential dependence of \bar{E} of I_B). It can be analysed only numerically. With the factor $\sigma(I_B, T_b, B)\alpha(I_B, \lambda, T_b, B)$ being independent of bias current, or if estimating it at inflection points of experimental curves is a good approximation, then the predicted *PCR* curves with any other parameters (T_b , λ , B) changing must exhibit parallel shifts along I_B axis. With a stronger non-linear dependence of the factor $\sigma(I_B, T_b, B)\alpha(I_B, \lambda, T_b, B)$ on I_B , the predicted *PCR* curves will exhibit changes of slopes of the rising parts with onsets at different bias currents. Moreover, in general $\sigma(I_B, T_b, B)\alpha(I_B, \lambda, T_b, B)$ is non-monotonic in the transition range. The four speculative patterns of *PCR* vs I_B can therefore be predicted as shown in Fig.3. While the pattern in Fig.3a is not uncommon, the pattern resembling Fig.3d was observed experimentally in narrow, $W=30$ nm, NbN SNSPDs²⁹.

D. The effect of Fano-fluctuations on the shape of *PCR* curves in wide SNSPDs

In wide SNSPDs, the sensor response depends on the y -coordinate of the absorption site across the nanowire. In a spatially homogeneous nanowire this dependence will affect the shape of the *PCR* curves in the transition region, reflecting the curvature of the predicted dependence of detection current vs coordinate y . Two shapes of $I_{det}(y, E, T_b, \lambda)$ are discussed in the literature: bell-shaped¹⁵ and w-shaped^{18,37}. Fig.4a shows schematically these I_{det} profiles. For illustration we will take the w-shaped profile depicted in Fig.4a with averaged detection current at one half and a difference between maximum and minimum detection currents of ~ 0.1 of the critical depairing current. We obtain the *PCR*-curve shown in Fig.4b. Fano-fluctuations will smear this curve. However, in order to evaluate this smearing, apart from the

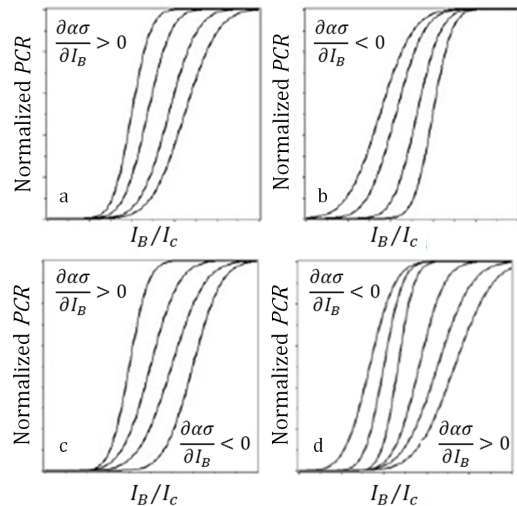


FIG. 3: Predicted patterns of *PCR* vs I_B

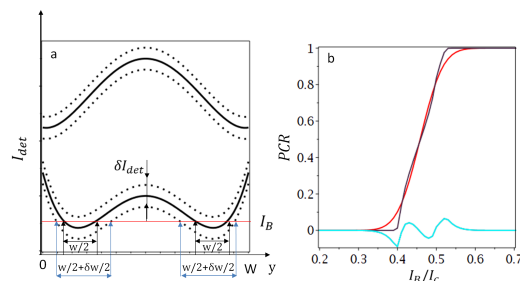


FIG. 4: a. Schematic profiles of I_{det} vs transverse coordinate y : top curve - bell shaped, bottom - w-shaped. b. *PCR* for w-shaped profile of I_{det} , best fit error function shape -red and difference between the two shapes -cyan

variance σ we must evaluate the sensitivity of $I_{det}(y)$ relative to fluctuations of the deposited energy, the derivative in the denominator in (9). This depends on the material properties and detection model. Instead, shown superimposed is the closest fit error function curve and difference between the two curves. As is seen, the difference between the two curves can be resolved experimentally allowing us to study the co-ordinate dependent response, on the background of either normally distributed static spatial inhomogeneities or dynamic Fano-fluctuations. Similarly, the distinguishing features of the *PCR* curve for the bell-shaped profile of detection current can also be resolved experimentally.

Observation of smooth error function-like sigmoidal shapes in wide-wire SNSPDs will indicate a much weaker co-ordinate dependence than shown in Fig.4a. Such a weak co-ordinate dependence on its own cannot be responsible for the observable width of the transition region, δI_B , $I_{det,max} - I_{det,min} \ll \delta I_B$. In this case the shapes of *PCR* curves of wide-wire SNSPDs will closely resemble *PCR* curves of narrow-wire SNSPDs. Spatial inhomogeneity connected to vortex initiation is totally

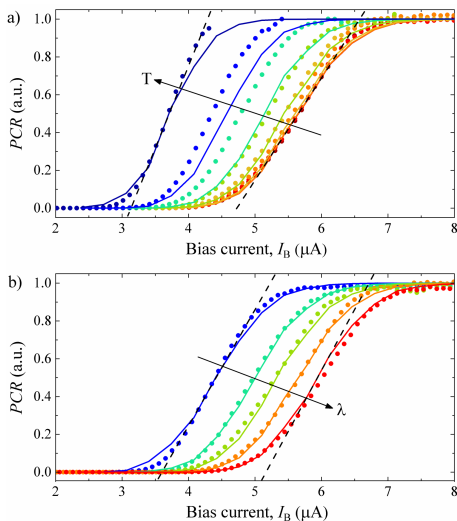


FIG. 5: Photon count rate (PCR) for a WSi SNSPD operated in the single-photon detection regime as a function of bath temperature a) from 250 mK to 2 K with the increment 250 mK and wavelength b) $\lambda=1200, 1350, 1450, 1550$ and 1650 nm. Solid curves-theoretical simulation, solid circles - experiment. Dashed lines indicate the slopes of the outer PCR curves

smearred by fluctuations, which also determine the width of the transition region, δI_B . Moreover, hot belt and hot spot models³⁷ will further merge with appropriate replacements $T_s \leftrightarrow T^*$, $I_{co} \leftrightarrow I_{det}$ and $\alpha(I_B, \lambda, T_b, B) \leftrightarrow I'_{det}(y, \chi E_\lambda, T_b, B, \lambda)$.

III. COMPARISON WITH EXPERIMENT

A. PCR vs I_B curves

For comparison with experiment, we have chosen the PCR vs I_B curves of WSi SNSPDs measured at different excitation wavelengths and bath temperatures³⁰ shown in Fig.5. To simulate these data we used the hotspot dynamics model developed in³¹, modified to include Fano fluctuations. In the absence of Fano fluctuations and spatial inhomogeneities this model predicts step-like PCR curves.

Fig.5a shows the experimental and fitted PCR vs I_B curves at different temperatures. The fitting parameters were the same as in Marsili et al³⁰ except for a higher photon yield $\bar{\chi} = 0.32$, allowing the switching current to be $\sim 60\%$ of the de-pairing current. In the absence of measurements of the de-pairing current, its value is an additional fitting parameter, allowing a better match between theory and experiment. For evaluation of σ_2 we used $J = 1.3$. The calculated values of J^1 for WSi on a-SiO₂ range between 0.5 to 1.5 (for $\eta = 0.5$) and 0.33 to 1.0 (for $\eta = 0.3$) taking τ_0 in the interval 2 to 10 ns. $l_{pe,D}$ varies in the limits from 0.8 nm for $\tau_0 = 2$ ns to 4 nm for $\tau_0 = 10$ ns. Note that there is no information in the litera-

ture about the strength of elastic scattering of phonons in amorphous WSi film. For comparison, in a 6.9 nm-thick amorphous SiO₂ film, the phonon mean free path defining heat conductivity at $T > 50$ K is comparable to film thickness³⁴. The qualitative agreement between theory and experiment in Fig.5a is good. The simulated curves for the whole range of bath temperatures from 0.25 to 2 K are close to experimental results, simulations also reproduce the steeper slopes of the PCR curves with increased bath temperature. This feature is clearly seen in the experimental data and is an extra consistency check of our kinetic model.

Also consistent with experimental data is the group of simulated PCR curves for different photon wavelengths at fixed bath temperature, which have almost identical slopes. We used the same set of fitting parameters as in Fig.5a, fixing the bath temperature and allowing λ to change. Steeper slopes at smaller bias currents (higher T_s in fixed- λ experiment) originate in the nonlinear $E(I_B, T_s, B) - E(I_B, T_b, B)$ dependence. The same nonlinearities are effective for similar range of currents determining the shape of PCR curves also for the second experiment, i.e. PCR vs bias current at fixed bath temperature and variable λ . However, in the second experiment, shown in Fig. 5b, the effect of nonlinearity is nearly balanced by the square root dependence of variance σ on photon energy. As a result the corresponding slopes remain almost unchanged, as expected from the model.

B. P_{click} vs t_D curves

We have shown that Fano fluctuations play an important role in smearing the detection threshold. This conclusion holds regardless of the ultimate detection mechanism, which primarily affects the magnitude of the threshold energy E^* and correspondingly the effective T_s . Here we discuss the role of Fano fluctuations in determining the hotspot relaxation dynamics. As reported in Ref.³⁰, we coupled optical pulse pairs separated by a variable delay t_D to an SNSPD operating in the two photon regime. In the two photon detection regime, a photoresponse pulse can be efficiently triggered only if two photons generate two overlapping hotspots. As shown in Fig.6, we measured the probability of a response pulse, or click (P_{click}), as a function of t_D for different bias currents. The P_{click} vs t_D curves have Lorentzian shape and become wider if the bias current is increased. We defined the hotspot relaxation time as the half width at half maximum of each Lorentzian curve. This profile is evidenced by the shape of the two-photon $PCR(t_D)$ as a function of time delay between two single-photon pulses³⁰.

In an idealized model with a sharp threshold for single-photon detection, P_{click} vs t_D curves will have a rectangular shape with a width determined by the hotspot relaxation time³¹. According to our model, Fano fluctuations smear the sides of these rectangular curves,

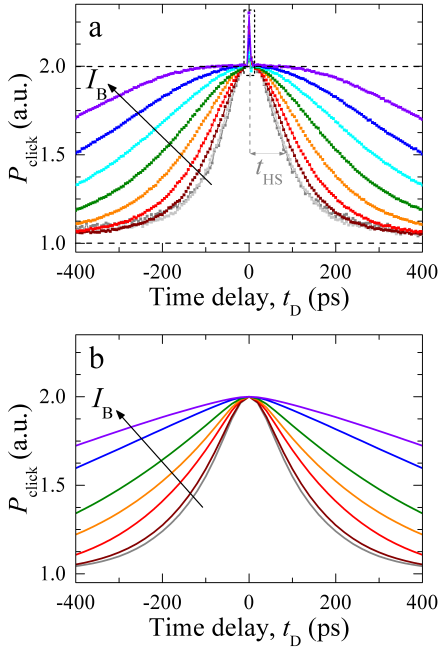


FIG. 6: PCR as a function of time delay t_D for a series of bias currents: (a) experiment, (b) theory.

transforming them to bell-shape curves. Neglecting diffusive expansion³¹, we let the first pulse at $t = 0$ deposit an energy E with probability $P(E)$, which creates a hotspot with initial temperature $T_{ex} = T(E, T_b, I_B)$. Subsequently the hotspot relaxes, and its temperature follows the functional dependence $T(E, T_b, I_B, t)$. The latter can be found as a solution of the kinetic equation³¹. At an instance of time $t = t_D$, the hotspot energy, E_{HS} , thus decreases to $E_{HS}(T(E), T_b, I_B, t_D)$. Then the normalized two-photon P_{click} becomes

$$PCR(t_D) = \int_0^\infty dEP(E) \int_{E^* - E(T(E), T_b, I_B, t_D)}^\infty dE' P(E') = \frac{1}{2} \int_0^\infty dEP(E) \operatorname{erfc} \left[\frac{E(I_B, T_s) - E(T(E), T_b, I_B, t_D) - \bar{E}}{\sqrt{2}\sigma} \right] \quad (12)$$

Fig.6b shows the simulated shapes of $P_{click}(t_D)$ for several different values of bias current using the following parameters, $J = 1.3$, $\bar{\chi} = 0.32$, $I_{sw}/I_{dep}=0.68$ and $\tau_0 = 5.0$ ns.

As expected, Fano fluctuations play a dominant role in shaping the photoresponse $P_{click}(t_D)$, also providing further evidence that in amorphous WSi nanowires hotspot relaxation proceeds via self-recombination. While the simulated curves in Fig.6 can be better matched to the experimentally observed Lorentzians over the hotspot lifetime defining range of time delays, their tails differ from experiment. The results of such a match are shown in Fig.7. The simulated tails fall between that of Lorentzian and Gaussian. It is possible that diffusion makes most of its contribution at

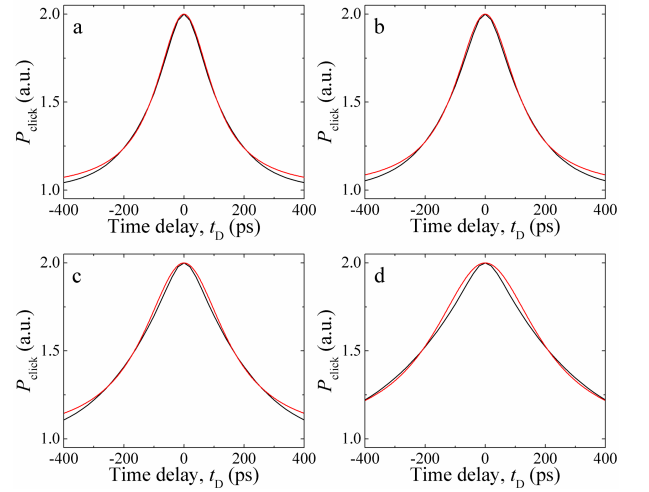


FIG. 7: Fitting the simulated $PCR(t_D)$ for series of bias currents by the Lorentzians.

the tails of $PCR(t_D)$, causing reduced self-recombination at the periphery of the hotspot. Simulations in Fig.6 look reasonably close to experimental curves. They were done at parameter values close to our of earlier work^{30,31} assuming switching current 32% less than de-pairing current and correspondingly more efficient energy deposition parameter. In general larger difference between the switching and de-pairing currents requires larger factors $\bar{\chi}$ to match theory and experiment. Physically that means that achieving the higher critical temperature in a wire with bias current being a smaller fraction of the de-pairing current requires more deposited energy. Also, decreasing I_{sw}/I_{dep} and increasing $\bar{\chi}$ results in a weaker dependence of hotspot relaxation time (half width at half maximum) on bias current as evidenced by a weaker dependence of hotspot relaxation time on I_B at lower currents. This dependence becomes weaker also for larger values of τ_0 . Allowing I_{sw}/I_{dep} to be free fitting parameter we may shift simulated PCR curves along the bias current axis achieving better fit to experiment. These simulations must be considered together with best fits in Fig.5 which required the same set of fitting parameters as for simulations in Fig.6 except for $I_{sw}/I_{dep}=0.6$. Achieving good fit with the same material parameters and fixed values for I_{sw}/I_{dep} , σ and $\bar{\chi}$ is very challenging. We could have fitted each separate experiment better allowing some flexibility of each individual parameter. The fact that we can semi-quantitatively fit all the different experiments, allowing 12% variation of a single I_{sw}/I_{dep} fitting parameter and keeping the rest the same, shows both the validity of the model and the accuracy of the main assumptions.

Simulation of $PCR(t_D)$ for two-photon detection with variable time delay requires the two additional parameters, τ_0 , determining the time scale, and cutoff temperature, determining the level of cooling of hotspot below which it cannot be detected at arrival of the second

photon. Both parameters are irrelevant for single photon detection. It is important to note that for a given photon wavelength the ratio of cutoff to critical temperature T_s is not an entirely independent parameter. It depends on the ratio of bias- to de-pairing currents. However, this dependence is highly non-linear and its effect on simulations differs from the linear scaling of the bias relative to de-pairing current, which is sufficient for fitting single photon counting rates. In two-photon experiments with variable time delay, both linear re-scaling of the bias relative to depairing current and nonlinearity of ratio of T_{co} to T_s are important, and hence credibility of both sets of simulations depends on assumed applicability of BCS model. Finally, the role of diffusion, which has not been discussed so far is also important. The simple model^{30,31}, although acknowledging its potential role, ignored it with some support from experimental data.

C. Discussion

Our simulations of single-photon *PCR*-curves and two-photon pump-and-probe experiments with variable time delay were based on a narrow nanowire hot-belt model. The analogous hot-belt model was claimed to be irrelevant for both NbN and WSi SNSPDs with nanowire width exceeding 150 nm³⁷. Our experiments and simulations therefore allow testing of the hot-belt model predictions for a wide range of experiments and comparison to predictions of the hotspot model where we can identify expected differences. The hot belt model is expected to work for the two-photon detection experiment. It was demonstrated to produce qualitatively similar but quantitatively strongly different results to the hotspot model (except for SNSPDs in external magnetic fields in a certain range of bias currents). In contrast, the agreement with both experiments that comes as the result of our analysis is much closer than what could have been inferred on assumption that hot-belt and hotspot models work for two-photon and one-photon experiments respectively.

The validity criterion for the narrow-wire model is $\tau_{th} \geq \tau_D$, where τ_{th} is the characteristic thermalisation time, controlling suppression of the gap within the initial volume, and τ_D is characteristic diffusion time across the nanowire³⁷. We do not use the coherence length as the radius R_0 of phonon bubble. This scale is not relevant for the initial state, because the radius of phonon bubble must be exactly the same for a normal metal. We chose $R_0 = \sqrt{4Dt_d + l_{pe,D}^2}$ as the more appropriate spacial scale. Here t_d stands for the descent time for photoelectron(hole) from the level E_1^* to Fermi energy. The meaning of R_0 is the length of the random walk, that the primary photoelectron and hole perform while disposing their excess energy to phonons, creating a phonon bubble. The second term under the square root accounts for extra volume expansion due to phonons of the bub-

ble moving on average a distance of their mean free path prior to being re-absorbed by electrons. For WSi using $d = 5$ nm, $D = 0.75\text{cm}^2/\text{s}$ ³⁰, $\tau_0 = 10$ ns, $\Omega_D = 34$ meV³⁹, $t_d = \tau_0 \frac{2E_1^*}{\Omega_D} \left(\frac{T_c}{\Omega_D} \right)^3$, $\tau_{pe,D} = \frac{\tau_0 T_c}{\gamma \Omega_D}$ and $\gamma=89$ we obtain for volume of phonon bubble $V_0 = \pi R_0^2 d = 2044$ nm³ exceeding initial volume used for the estimate of τ_{th} in ref.³⁷. Correspondingly, the energy density is smaller resulting in lower temperature of electrons and phonons in the hotspot $T_e = T_{ph} = 4.1T_c$ and $\tau_{th}=8.7$ ps for absorption of a 1550 nm photon as estimated from energy conservation. There is currently no consensus in the literature regarding the magnitude of τ_0 with recent measurements of magnetoresistance³⁸ yielding $\tau_0=1.9$ ns. We have chosen $\tau_0=10$ ns for two reasons. It fits the measurements of electron-phonon relaxation time³⁹ over the low temperature range. It also better fits the expected magnitude of τ_0 inferred from scaling according to Ω_D^2/T_c^3 law, which must work during the formation of phonon bubble when effects of disorder on electron-phonon interactions are not important. Phonon escape from the SNSPD film and diffusive expansion during thermalisation both reduce the energy density within the volume filled with non-equilibrium excitations resulting in further slowdown of thermalization. A more important process is likely to be diffusive expansion, which may result in a substantial increase of τ_{th} . Indeed, during the first picosecond evolving hotspot with the initial volume of 2044 nm³ expands to fill the volume of 4700 nm³. Reducing energy density within the evolving hotspot results in the temperature of thermalised quasiparticles and phonons of $3.1T_c$ and $\tau_{th} > 19.0$ ps (>9.5 ps if to assume $\tau_0=5$ ns). The representative value for expansion time of hotspot across the width of the wire is the diffusion time from the centre of the strip, $\tau_D \sim W^2/16D \simeq 14.1$ ps. The account of both phonon loss and diffusion during the stage of thermalisation must be done within the refined model. In the absence of such a model and in view of significant uncertainty of material parameters the question of validity of one or the other model remains open.

The experimental data in Figs.5a and b have smooth sigmoidal shapes close to predicted error functions. Indeed, there is no evidence of coordinate-dependent response in the transition region. With any of the bell or w-shaped coordinate-dependent responses, one expects the specific change of curvature at the inflection point from concave below, $I_B < I_{co}$, to convex above cutoff current, $I_B > I_{co}$ as shown in Fig.4. In contrast, for a narrow wire, the predicted error function shape is convex on the left and concave on the right of the inflection point, I_{co} . In order to check whether the experimental curves in Fig.5 can be approximated by error functions in Fig.8 we show the results of matching the curves from Fig.5 to error functions, $PCR = \frac{A}{2} \text{erfc} \left(\frac{I_{co} - I_B}{\Delta I} \right)$, where A and ΔI are fitting parameters. No clear signs of coordinate-dependent response are seen in Fig.8.

In a recent paper on MoSi SNSPDs, the *PCR* curves

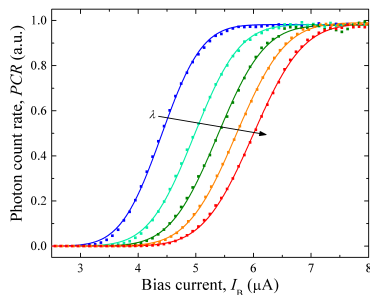


FIG. 8: Fitting PCR vs I_B for $\lambda = 1200, 1350, 1450, 1550$ and 1650 nm by error functions.

were measured and fitted with error functions for a wavelength range of 750 to 2050 nm. It was found that at low photon energies the fit agrees very well with the data. However, at high energies, the shape of the curves starts to deviate from simple error function⁴⁰. The authors hypothesize that these deviations might indicate a coordinate-dependent response of the SNSPD. The observed deviations, however, are not what can be expected from coordinate-dependent response. Firstly, the curvatures of PCR -shapes on both sides of inflection points remain consistent with fluctuation-induced homogeneous sensor response. Secondly, the experimental curve shows smaller counts both in the lower bias tail and on approach to saturation level. This is not indicative of an inhomogeneous response, for which on approach to I_{det}^{max} photon counting rate must exhibit a discontinuity in its derivative. It is possible that the observed deviations are connected with non-linearity of SNSPD response as given by the function α in expression (11). This non-linearity is of the same origin as the observed substantial non-linearity of current-energy relation in MoSi⁴⁰. These results may be also explained within the hotspot model provided that detection current is only weakly dependent on coordinates of absorption site so that predictions of hotspot model for the shape of PCR vs I_B will be no different and both models further merge as explained in Section II.

The effects of an external magnetic field on PCR vs bias current^{17,22,35,36} deserve special attention, since they can give insight into the detection mechanisms in SNSPDs^{22,35}. Features due to Fano fluctuations were not accounted for in any of the previous work. There are several ways that external magnetic fields can combine with Fano fluctuations and thus cause the PCR curves to change shape. In an external perpendicular magnetic field, the threshold E^* depends on the field magnitude, as seen in (5) and (8). Both the critical current and the de-pairing energy depend on magnetic field, with the former being dominant for weak magnetic fields. With

$I_c(B)$ decreasing, while B increases, the obvious effect in weak fields is the shift of PCR curves towards lower currents, as observed in^{22,35,36}. The magnitude of the shifts depends on the exact functional dependence of $I_c(B)$.

Vodolazov et al^{22,35} observed shape transformations of the PCR curves with varying magnetic field and photon wavelength above the crossover current. Their results were interpreted on the basis of a model assuming vortex trapping by compact hotspots having a radius depending on the photon wavelength. The SNSPD response in a weak magnetic field was suggested as the definitive experiment for identification of the detection mechanism³⁷. Within our model with uniform current density, there is no such a crossover. Nonetheless, the shifts may assume a more complicated pattern due to the interplay between the critical current, the de-pairing energy, and the complicated nonlinear $E(I_B, T_s, B) - E(I_B, T_b, B)$ dependence. At shorter photon wavelengths, the PCR curves shift towards lower bias, where the contribution of magnetic field term to de-pairing energy increases relative to the supercurrent term. Significant non-linearity of the energy-current relation was recently reported over the spectral interval 750-2050 nm⁴⁰. A full understanding of the detection mechanisms in SNSPDs will require a more detailed study of PCR shapes through the transition range at the low current tail, near inflection point(s) and close to saturation together with thorough study of the role of magnetic field affecting non-linearities of response and Fano effect.

IV. CONCLUSIONS

In summary, we have shown that Fano fluctuations play a fundamental role in superconducting nanowire single-photon detectors. They are an essential factor in determining the exact shape of both single-photon photoresponse and time-delayed, two-photon photoresponse. The special features of $PCR(I_B)$ curves, such as slope transformation, positions of inflection point(s) versus wavelength, bath temperature and magnetic field reveal a wealth of sensor physics and will do a significant service for unambiguous determination of the detection mechanism(s).

V. ACKNOWLEDGEMENTS

AGK and CL acknowledge financial support from the Engineering and Physical Sciences Research Council. AGK, FM and MDS acknowledge financial support from DARPA, J.P.A. was supported by a NASA Space Technology Research Fellowship.

-
- ¹ R. T. Williams, J. Q. Grim, Qi Li, K. B. Ucer, G. A. Bizarri and A. Burger, Scintillation Detectors of Radiation: Excitations at High Densities and Strong Gradients in "Excitonic and Photonic Processes in Materials" ed. Jai Singh and Richard T. Williams, Springer Series in Materials Science 203 (2015)
- ² K. J. Tielrooij, J. C. W. Song, S. A. Jensen, A. Centeno, A. Pesquera, A. Zurutuza Elorza, M. Bonn, L. S. Levitov and F. H. L. Koppens, Photoexcitation cascade and multiple hot-carrier generation in graphene, Nature Physics **9**, 248252 (2013)
- ³ Justin C. W. Song, Leonid S. Levitov, Energy Flows in Graphene: Hot Carrier Dynamics and Cooling, J. Phys.: Condens. Matter **27**, 164201 (2015)
- ⁴ J. Janesick, T. Elliott, R. Bredthauer, C. Chandler, B. Burke, "Fano fluctuations-Limited CCDs", Proc. SPIE, **0982**, 70 (1988).
- ⁵ G.F. Knoll, Radiation Detection and Measurement, fourth ed., Wiley and Sons, 2010.
- ⁶ M.Kurakado, Possibility of high resolution detectors using superconducting tunnel junctions, Nucl. Instr. Meth. **196**, 275(1982)
- ⁷ N.Rando, A.Peacock, A. van Dordrecht *et al*,The properties of niobium superconducting tunneling junctions as X-ray detectors, Nucl. Instr. Meth A **313**, 173 (1992).
- ⁸ B. Cabrera, R. M. Clarke, P. Colling, A. J. Miller, S. Nam, and R. W. Romani, Detection of single infrared, optical, and ultraviolet photons using superconducting transition edge sensors Appl. Phys. Lett. **73**, 735 (1998).
- ⁹ D.D.E. Martin, P. Verhoeve, A. Peacock, A.G. Kozorezov, J.K. Wigmore, H. Rogalla, R. Venn, Resolution limitation due to phonon losses in superconducting tunnel junctions, Appl.Phys. Lett. **88**, 123510 (2006).
- ¹⁰ 38. Kozorezov, A. G. Wigmore, J. K. Martin, D. Verhoeve, P.; Peacock, A., Resolution limitation in superconducting transition edge photon detectors due to downconversion phonon noise, Applied Physics Letters, **89**, 223510 (2006).
- ¹¹ A.G. Kozorezov, C.J.Lambert, S.R. Bandler, M.A. Balvin, S.E. Busch, P.N. Nagler, J-P. Porst, S.J. Smith, T.R. Stevenson, J.E. Sadleir, Athermal energy loss from x-rays deposited in thin superconducting films on solid substrates, Phys. Rev. B **87**, 104504 (2013).
- ¹² A.E. Lita, A.J. Miller, S. Nam, Energy Collection Efficiency of Tungsten Transition-Edge Sensors in the Near-Infrared, J Low Temp Phys, **151**, 125 (2008).
- ¹³ A. D. Semenov, et al., "Quantum detection by current carrying superconducting film" Physica C **351**, 349 (2001).
- ¹⁴ A. Semenov, et al., "Spectral cut-off in the efficiency of the resistive state formation caused by absorption of a single-photon in current-carrying superconducting nano-strips" Eur. Phys. J. B **47**, 495 (2005).
- ¹⁵ A.Engel,J.Lonsky,X.Zhang, Detection Mechanism in SNSPD: Numerical Results of a Conceptually Simple, Yet Powerful Detection Model, IEEE Ttans. Appl, Superconductivity, **25**, 2200407 (2015)
- ¹⁶ L. N. Bulaevskii, M. J. Graf, C. D. Batista, and V. G. Kogan,Vortex-induced dissipation in narrow current-biased thin-film superconducting strips, Phys. Rev. B **83**, 144526 (2011).
- ¹⁷ L. N. Bulaevskii, M. J. Graf, and V. G. Kogan, Vortex-assisted photon counts and their magnetic field dependence in single-photon superconducting detectors, Phys. Rev. B **85**, 014505 (2012).
- ¹⁸ D.Yu. Vodolazov, Current dependence of the red boundary of superconducting single-photon detectors in the modified hot-spot model, Phys. Rev. **B** **90**, 054515 (2014)
- ¹⁹ A. N. Zotova and D. Yu. Vodolazov, Intrinsic detection efficiency of superconducting nanowire single photon detector in the modified hot spot model, Supercond. Sci. Technol. **27** 125001 (2014)
- ²⁰ J. J. Renema, R. Gaudio, Q. Wang, Z. Zhou, A. Gaggero, F. Mattioli, R. Leoni, D. Sahin, M. J. A. de Dood, A. Fiore, and M. P. van Exter, Experimental Test of Theories of the Detection Mechanism in a Nanowire Superconducting Single Photon Detector, PRL, **112**, 117604 (2014)
- ²¹ A.Engel, J.J.Renema, K.Ilin, A. Semenov, Detection mechanism of superconducting nanowire single-photon detectors, Supercond. Sci. Technol. **28**, 114003 (2015).
- ²² D. Yu.Vodolazov, Yu. P.Korneeva, A. V.Semenov, A. A.Korneev, G. N.Goltsman, Vortex-assisted mechanism of photon counting in a superconducting nanowire single-photon detector revealed by external magnetic field, Physical Review **B92**, 104503(2015)
- ²³ A.G. Kozorezov, A.F. Volkov, J.K. Wigmore, A. Peacock, A. Poelaert, R. den Hartog, Quasiparticle-phonon downconversion in nonequilibrium superconductors, Phys. Rev. **B61**, 11807 (2000).
- ²⁴ B.L.Altshuler and A.G.Aronov in "Electron-electron Interactions in Disordered systems", ed. by A.L.Efros and M.Pollak, Elsevier Science Publishers B.V., 1985
- ²⁵ J-J Chang in "Nonequilibrium Superconductivity" ed. by D.N.Langenberg and A.I.Larkin, Elsevier Acince Publishers B.V. 1986
- ²⁶ A.Schmid, Electron-phonon interaction in an impure metal, Z. Phys. **259**, 421 (1973)
- ²⁷ M. Yu. Reizer and A. V. Sergeev, The effect of the electron-phonon interaction of the conductivity of impure metals , Sov. Phys. JETP **65**, 1291 (1987)
- ²⁸ S.B. Kaplan *et al*, Quasiparticle and phonon lifetimes in superconductors, Phys.Rev. B **14**, 4854 (1976)
- ²⁹ F. Marsili, F. Bellei, F. Najafi, A. Dane, E. Dauler, R. Molnar, and K. Berggren, Efficient Single Photon Detection from 500 nm to 5 m Wavelength, Nano Lett., **12**, 4799 (2012)
- ³⁰ F. Marsili, M. J. Stevens, A. Kozorezov, V. B. Verma, Colin Lambert, J. A. Stern, R. D. Horansky, S. Dyer, S. Duff, D. P. Pappas, A. E. Lita, M. D. Shaw, R. P. Mirin, and S. W. Nam, Hotspot relaxation dynamics in a current-carrying superconductor, Phys. Rev. B **93**, 094518 (2016)

- ³¹ A.G.Kozorezov, C. Lambert, F. Marsili, M. J. Stevens, V. B. Verma, Colin Lambert, J. A. Stern, R. Horansky, S. Dyer, M. D. Shaw, R. P. Mirin, and S. W. Nam, Quasiparticle recombination in hotspots in superconducting current-carrying nanowires, *Physical Review B* **92**, 064504 (2015)
- ³² A. Anthore, H. Pothier, and D. Esteve, Density of States in a Superconductor Carrying a Supercurrent, *PRL* **90**, 127001 (2003)
- ³³ A.G. Kozorezov, J.K.Wigmore, D. Martin, P. Verhoeve, A. Peacock, Electron energy down-conversion in thin superconducting films, *Phys. Rev.B* **75**, 094513 (2007).
- ³⁴ E. T. Swartz, R. O. Pohl, Thermal boundary resistance, *Reviews of Modern Physics*, **61**, 605 (1989)
- ³⁵ A. A. Korneev, Y. P. Korneeva, M. Y. Mikhailov, Y. P. Pershin, A. V. Semenov, D. Y. Vodolazov, A. V. Divochiy, Y. B. Vakhtomin, K. V. Smirnov, A. G. Sivakov, A. Y. Devizenko, and G. N. Goltsman, Characterization of MoSi Superconducting Single-Photon Detectors in the Magnetic Field, *IEEE Transactions on Applied Superconductivity*, **25**, 6975120 (2015).
- ³⁶ J. J. Renema, R. J. Rengelink, I. Komen, Q. Wang, R. Gaudio, K. P. M. opt Hoog, Z. Zhou, D. Sahin, A. Fiore, P. Kes, J. Aarts, M. P. van Exter, M. J. A. de Dood, and E. F. C. Driessen, The effect of magnetic field on the intrinsic detection efficiency of superconducting single-photon detectors, *Appl. Phys. Lett.* **106**, 092602 (2015).
- ³⁷ D.Vodolazov, Theory of single photon detection by 'dirty' current-carrying superconducting strip based on the kinetic equation approach, arXiv:1611.06060 (2016)
- ³⁸ X.Zhang,A.Engel,Q.Wang,A.Schilling,A.Semenov,M.Sidorova,H.-W.Hbers,I.Charaev,K.II'in, and M.Siegel, Characteristics of superconducting tungsten silicide W_xS_{1-x} for single photon detection, *Phys.Rev.B* **94**, 174509 (2016)
- ³⁹ M.Sidorova, A.Semenov, A.Korneev, G.Chulkova, Yu.Korneeva, M.Mikhailov, A.Devizenko, A.Kozorezov, G.Goltsman, Electron-phonon relaxation time in ultrathin tungsten silicon film, arXiv:1607.07321
- ⁴⁰ Misael Caloz, Boris Korzh, Nuala Timoney, Markus Weiss, Stefano Gariglio, Richard J. Warburton, Christian Schonenberger, Jelmer Renema, Hugo Zbinden, and Felix Bussi'eres, Optically probing the detection mechanism in a molybdenum silicide superconducting nanowire single-photon detector, arXiv:1611.08238